H₂S alleviates renal injury and fibrosis in response to unilateral ureteral obstruction by regulating macrophage infiltration via inhibition of NLRP3 signaling

Yueyuan Zhou[a,1], Xiaoyan Zhu[d,1], Xuan Wang[a], Yi Peng[a], Jiankui Du[b,d], Hongling Yin[c], Hui Yang[a], Xin Ni[b,d,*], Weiru Zhang[a,**]

[a] Department of Rheumatology and Immunology, Xiangya Hospital, Central South University, Changsha, Hunan, China
[b] National International Joint Research Center for Medical Metabolomics, Xiangya Hospital, Central South University, Changsha, Hunan, China
[c] Department of Pathology, Xiangya Hospital, Central South University, Changsha, Hunan, China
[d] Department of Physiology, Second Military Medical University, Shanghai, China

ARTICLE INFO

ABSTRACT

Renal fibrosis is a key pathological feature in chronic kidney diseases (CKDs). Dysregulation of hydrogen sulfide (H₂S) homeostasis is implicated in the pathogenesis of CKDs. Here, C57/BL6 mice were allocated to Sham and unilateral ureteral obstruction (UUO) groups, which were treated with NaHS or NLRP3 inflammasome inhibitor 16673-34-0 for 3–14 days. UUO mice displayed downregulation of H₂S production and increased macrophage infiltration in obstructed kidneys. H₂S donor NaHS treatment attenuated renal damage and fibrosis and inhibited M1 and M2 macrophage infiltration. NLPR3 inflammasome was activated and levels of phosphorylated nuclear factor κB (NF-κB) p65 subunit, phosphorylated signal transducer and activator of transcription 6 (STAT6) and interleukin (IL)-4 protein were increased in the kidneys after UUO. NLRP3 inhibitor inactivated NF-κB and IL-4/STAT6 signaling, suppressed M1 and M2 macrophage infiltration and attenuated renal damage and fibrosis in UUO mice. NaHS treatment also suppressed NLRP3, NF-κB and IL-4/STAT6 activation in the obstructed kidneys. In conclusion, the therapeutic effects of H₂S on UUO-induced renal injury and fibrosis are at least in part by inhibition of M1 and M2 macrophage infiltration. H₂S suppresses NLRP3 activation and subsequently inactivates NF-κB and IL-4/STAT6 signaling, which may contribute to the anti-inflammatory and anti-fibrotic effects of H₂S.

1. Introduction

Renal fibrosis is a final common pathway leading to end-stage kidney failure in many chronic kidney diseases (CKDs) [1,2]. Among the diverse causative factors, interstitial macrophage accumulation has been recognized as an important component of CKD that contributes to disease progression and fibrosis [3]. Macrophages are heterogeneous, multifunctional immune cells that can be broadly divided into two categories based on their response to different microenvironments: classically activated inflammatory macrophages (M1) and alternatively activated macrophages (M2). M1 macrophage activation is associated with tissue destruction and inflammation and is characterized by increased production of proinflammatory cytokines, nitric oxide and reactive oxygen species. In contrast, M2 polarized macrophages typically have immune-suppressive activity and express arginase (Arg)-1, promoting tissue repair and collagen production [4,5]. Accumulating evidence suggests that subsets of M1 and M2 macrophages are likely to coexist during the pathogenesis of renal fibrosis [6]. Controlling the infiltration of M1 and M2 macrophages may represent a potential therapeutic strategy for preventing renal fibrosis.

M1/M2 polarization of macrophage is a tightly controlled process entailing a set of signaling pathways and transcriptional regulatory networks. As a key transcription factor related to pro-inflammatory processes, nuclear factor κB (NF-κB) activation modulates M1 polarization that is activated by Toll ligand receptor (TLR) ligands [7,8]. and regulates the expression of a large number of inflammatory genes including tumor necrosis factor (TNF)-α, interleukin (IL)-1β, interleukin (IL)-6, and inducible nitric oxide synthase (iNOS). On the other hand,

activation of the interferon regulatory factor/signal transducer and activator of transcription (IRF/STAT, via STAT6) signaling pathways by IL-4 and IL-13 skews macrophage function toward the M2 phenotype [9,10].

The central inflammasome component NACHT, LRR, and PYD domains-containing protein 3 (NLRP3) form a cytosolic multimolecular platform in complex with the adaptor protein ASC and caspase-1 and activates caspase-1, which, in turn, proteolytically matures and leads to the release of bioactive IL-1β and IL-18 [11]. NLRP3 is known to mediate NF-κB activation in a variety of cell types [12,13]. Activation of NLRP3 inflammasome plays a critical role in M1 macrophage polarization [8,14]. Moreover, NLRP3 also acts as a key transcription factor to transactivate IL-4 promoter [15], and is found to regulate M2 macrophage polarization through the up-regulation of IL-4 in asthma [9]. Previous studies have shown that the NLRP3 inflammasome is involved in the pathogenesis of renal inflammation and CKD [16,17]. However, whether NLRP3 activation contributes to the increased infiltration of M1 and M2 macrophages in CKD remains largely unknown.

Hydrogen sulfide (H_2S) is now considered as the third gas transmitter after nitric oxide (NO) and carbon monoxide (CO) [18]. Two key enzymes that catalyze the production of H_2S, cystathionine-β-synthase (CBS) and cystathionine-γ-lyase (CSE) are enriched in proximal renal tubules and produce H_2S through the transsulfuration pathway [19]. Dysregulation of H_2S homeostasis is implicated in the pathological processes of renal inflammation and CKD [20–23]. H_2S treatment can attenuate the activation of NLRP3 inflammasome and NF-κB pathways in multiple cell types including macrophages [24–26]. These findings raise an intriguing possibility that H_2S may regulate the infiltration of M1 and M2 macrophages in CKD via modulating NLRP3-dependent signal pathways in renal tissues.

In the present study, we investigated the effect of H_2S on macrophage infiltration, tissue damage and fibrosis in obstructed kidneys of unilateral ureteral obstructive (UUO) mice. Given that M1 and M2 macrophage infiltration contributes to UUO-induced fibrosis [27–29], we then examined the effects of H_2S on M1 and M2 macrophage infiltration. Finally, we explored whether NLRP3-dependent signaling pathways were involved in the protective effects of H_2S against UUO-induced macrophage infiltration, tissue damage and fibrosis.

2. Materials and methods

2.1. Animal surgery and experimental protocols

Wild-type 9-week-old male C57BL/6 mice (22–25 g) were purchased from SLAC Laboratories (Changsha, China). Mice were housed in the animal care facility of the Xiangya Medical College of Central South University and had access to food and water ad libitum for the duration of the study. All protocols involving animals were reviewed and approved by the institutional animal welfare committee of Central South University. We performed sham surgery (free ureter) or unilateral ureteral obstruction in mice. UUO was induced by ligation of the left ureter according to the procedure previously described [30]. First, we randomly assigned C57BL/6 mice into eight groups (6 mice per group): four groups (Sham, UUO3d, UUO7d, and UUO14d) were treated with NaHS [19] (Sigma-Aldrich, St. Louis, MO, USA, 50 μg/kg/d, ip) or an equal amount of saline. Second, we randomly divided C57BL/6 mice into four groups (6 mice per group): mice after sham and UUO surgery were injected intraperitoneally with the vehicle (5%DMSO + 40% PEG300 + 5%Tween80 + ddH$_2$O) or a specific NLRP3 inhibitor 16673-34-0 (Selleck Chemicals, Houston, USA) [31] at 10 mg/kg once daily for 7 days.

2.2. Measurement of endogenous H_2S production

Endogenous H_2S production in renal tissues was measured as described previously [32]. Fresh kidney tissues were homogenized in cold PBS buffer (PH = 7.0). The lysate (80 μl) was mixed with 2 mmol/L L-cysteine, 2 mmol/L pyridoxal 5′-phosphate, and 100 mmol/L KH$_2$PO$_4$ buffer (pH = 6.8) with a final reaction volume of 1 ml in an Eppendorf tube sealed with Parafilm. After incubation at 37 °C for 1 h, the reaction was stopped on ice. Then, 10% ZnAc (500 μl) was injected into the Eppendorf tube using a sterile syringe to trap H_2S, before immediately sealing the hole with Parafilm. After incubation at room temperature for 10 min, the contents of the Eppendorf tubes were transferred into test tubes. *N,N*-dimethyl-*p*-phenylenediamine (Sigma-Aldrich, 2.4 mmol/L) in 7.2 M HCl and 4.5 mmol/L FeCl$_3$ in 1.2 M HCl was added. Twenty minutes later, the absorbance of the resulting solution at 670 nm was measured. For each experiment, an internal control reaction with ZnAc omitted was performed, for subtraction to obtain the H_2S-specific signal.

2.3. Immunofluorescence staining

For immunofluorescence staining, kidneys were snap frozen and embedded into optimum cutting temperature formulation (Sakura Finetek, Staufen, Germany). Cryosections of 8 μm thickness were prepared using Leica Cryostat CM3050 (Wetzlar, Germany) and were placed on silan-coated cover slides. Frozen sections were fixed and incubated overnight at 4 °C with antibodies against F4/80 (Abcam, Cambridge, MA, USA) at 1:100 dilution, CD206 (R&D Systems, Minneapolis, MN) at 1:150 dilution, and iNOS (Servicebio, Wuhan, China) at 1:500 dilution. Following incubation with CY3- or FITC-conjugated secondary antibodies (1:200, Abcam) for 1 h in the dark, the nucleus was stained with DAPI (Servicebio, Wuhan, China) for 5 min before microscopic analysis (Leica DFC500, Wetzlar, Germany). As a negative control, the primary antibodies were replaced by preimmune IgG from the same species; little or no nonspecific staining occurred. Quantification of the F4/80 positive areas was performed by taking random images (original magnification power × 400, 5 fields per kidney) of kidney sections from each mouse (n = 6) and counting the percentages of the positively stained areas in every microscopic field [28]. For the quantification analysis of double immunofluorescence staining, five high-power fields were analyzed in kidney sections taken from each mouse. We then determined the percentages of iNOS$^+$/F4/80$^+$ and CD206$^+$/F4/80$^+$ cells in total F4/80$^+$ cells, respectively.

2.4. Histopathological assessment

Formalin-fixed kidneys were embedded in paraffin and prepared in 4 μm sections for hematoxylin-eosin (HE) and Masson trichrome staining. The tubulointerstitial damage index and tubulointerstitial fibrosis score were graded as previously described [33].

2.5. Western blot analysis

Kidney tissues were homogenized in cold RIPA buffer (Beyotime, Jiangsu, China) containing 1% proteinase Inhibitor Cocktail (Sigma-Aldrich). 30 μg of protein were separated by 10% SDS-PAGE and subsequently transferred to PVDF membranes (Millipore Crop, Bedford, MA). Membranes were then blocked in Tris-buffered saline containing 0.1% Tween-20 (TBST) and 5% skimmed milk powder for 1.5 h at room temperature. Membranes were incubated with primary antibody against GAPDH (1:1000, Santa Cruz Biotechnology, Santa Cruz, CA, USA), CBS (1:500, Abcam), CSE (1:900, Abcam), NLRP3 (Cell Signaling Technology, Beverley, CA), NF-κB p65 (1:1000, Abcam), Phospho-p65 (1:1000, Cell Signaling Technology), Caspase-1/p20/p10 (1:600, Proteintech Group, Wuhan, China), STAT6 (1:1000, Cell Signaling Technology), Phospho-STAT6 (1:1000, Cell Signaling Technology) at 4 °C overnight, followed by incubation with a secondary HRP-conjugated IgG (1:1000, Santa Cruz) for 1 h at room temperature. Immunoreactive proteins were visualized using the 5200-ECL Chemiluminescence imaging system (Tanon, Shanghai, China). The

staining intensity of the bands was measured using ImageJ software.

2.6. Measurement of IL-4, serum creatinine (Scr) and blood urea nitrogen (Bun)

IL-4 in obstructed renal tissue was detected by ELISA kits (CUSABIO, Wuhan, China). Mouse serum creatinine and blood urea nitrogen concentrations were detected with an automatic biochemical analyzer (AU5400, Olympus, Tokyo, Japan).

2.7. Real-time qPCR analysis

Total RNA was extracted from kidney tissue using Trizol (Life Technologies, USA) reagent according to the manufacturer's instructions. The cDNAs were synthesized from 1 μg of the total RNA in a 20 μl reaction system using a PrimeScript™ RT reagent Kit (TaKaRa, Tokyo, Japan). The qPCR quantitation for individual target mRNA expression was performed with a QuantStudio 7 Real-Time PCR detection biosystem using a cDNA synthesis kit (GeneCopoeia, Guangzhou, China). The amount of specific mRNA in each sample was calculated based on the cycle threshold (CT) values, which were standardized with the quantity of the housekeeping gene GAPDH. Further calculation and statistical analysis were based on the comparative $2^{-\Delta\Delta CT}$ method. The primers used in the PCR reactions are listed in Supplementary Table 1.

2.8. Statistical analysis

Data were expressed as mean ± SEM. SPSS 20 (IBM, NY, USA) and GraphPadPrism 5 (GraphPad Software, CA, US) were used to perform statistical analyses and to build the graphs presented in this paper, respectively. Statistical comparisons between two groups were determined by two-tailed Student's t-test. One-way ANOVA with Bonferroni's post hoc test was performed for comparisons among multiple groups. A value of $p < 0.05$ was considered statistically significant.

3. Results

3.1. Downregulation of H₂S production is associated with increased macrophage infiltration in obstructed kidneys of UUO mice

To investigate the relationship between endogenous H_2S production and macrophage infiltration during the development of renal injury, we performed UUO surgery on mice and sacrificed mice 3, 7, and 14 days after surgery. As shown in Fig. 1A, there were very few F4/80-positive staining cells in the renal tissues of the sham group. Then 3, 7, and 14 days after ureteral ligation, mice that underwent UUO developed severe infiltration of F4/80$^+$ cells. The quantification analysis showed that the staining area of F4/80$^+$ cells was increased to 3.7%, 6.2% and 7.4% at 3, 7, 14 days after ureteral ligation, respectively (Fig. 1B). It was found that ureteral ligation resulted in decreased levels of kidney H_2S in a time-dependent manner (Fig. 1C), which were accompanied by time-dependent decreases in renal CSE and CBS expression (Fig. 1D). Notably, levels of H_2S were negatively correlated with F4/80$^+$ macrophage infiltration (Fig. 1E). These results indicate that CSE/CBS-mediated H_2S production is intimately linked with increased macrophage infiltration in the UUO model.

3.2. H₂S donor attenuates macrophage infiltration, tissue damage and fibrosis in the obstructed kidneys of UUO mice

We then examined the effect of H_2S donor, NaHS, on UUO-induced macrophage infiltration, tissue damage and fibrosis in the kidney. It was found that NaHS treatment [19] at a dose of 50 μg/kg/d for 7 and 14 days markedly reduced the number of F4/80$^+$ macrophages in the interstitium of obstructed mouse kidneys (Fig. 2A and B, Fig. 2B have

used the same control values as Fig. 1B). As shown in Fig. 2C and D, histologic examination with hematoxylin-eosin (HE) staining revealed progressive tubular dilation, tubular atrophy in the obstructed kidneys, simultaneously accompanied by inflammatory cell infiltration, with the renal tubulointerstitial injury scores of 4.7, 7.2, and 9.0 at 3, 7, 14 days after UUO, respectively. However, histological damage to the renal interstitium was alleviated by NaHS treatment, and the renal tubulointerstitial injury scores were reduced to 5.8 ($p < 0.05$), and 6.2 ($p < 0.001$) at 7 and 14 days after NaHS treatment, respectively.

Masson's trichrome staining demonstrated an increase of collagen deposition (blue area) as early as 3 days after UUO (Fig. 2E). After day 7, the collagen deposition appeared diffusively in the renal interstitium and was accompanied with dilatation of tubules and increases of interstitial cell number in the kidney. NaHS treatment at a dose of 50 μg/kg/d for 7 ($p < 0.01$) and 14 ($p < 0.001$) days markedly attenuated the fibrotic lesions with less collagen deposited in the renal interstitium (Fig. 2F).

In line with the morphological and histopathological data, the serum parameters for kidney failure and injury, Scr and Bun were also less severe in UUO mice treated with NaHS for 7 and 14 days as compared with saline-treated UUO mice (Fig. 2G and H).

3.3. H₂S inhibits M1 and M2 macrophage infiltration in the obstructed kidneys of UUO mice

Previous studies have shown that UUO-induced tubulointerstitial inflammation and fibrosis are accompanied by increased infiltration of both M1 and M2 macrophages [27–29], which can mediate renal injury and tissue repair, respectively. We then examined the effect of the H_2S donor on M1 and M2 macrophage infiltration in UUO kidneys. M1 phenotype was evaluated by iNOS expression, which was significantly increased in F4/80$^+$ infiltrating macrophages on saline-treated UUO kidneys. The quantification analysis showed that the percentage of iNOS$^+$/F4/80$^+$ cells in total F4/80$^+$ cells was induced as early as 3 days after UUO and reached the peak at 14 days post-obstruction, whereas administrating NaHS for 7 or 14 days resulted in a significant inhibition ($p < 0.001$) of M1 macrophage infiltration (Fig. 3A and B). Accordingly, the mRNAs of Rantes, TNF-α, IL-1β and IL-6 (M1 markers) are highly expressed in saline-treated UUO kidneys at 14 days post-obstruction, but the expression is significantly lower in NaHS-treated UUO kidneys (Fig. 3C–F).

In parallel, the M2 phenotype was evaluated by CD206 staining on renal sections. It was found that the percentage of CD206$^+$/F4/80$^+$ cells in total F4/80$^+$ cells was significantly elevated in kidneys at day 7 and day 14 after UUO, whereas administrating NaHS for 7 ($p < 0.01$) or 14 ($p < 0.05$) days resulted in a significant inhibition of M2 macrophage infiltration (Fig. 4A and B). In addition, UUO-induced mRNA expressions of CD206, Arg-1, and tissue inhibitor of metalloproteinases 1 (TIMP-1) (M2 markers) in renal tissues were significantly inhibited by NaHS treatment for 14 days (Fig. 4C, D and E). Taken together, these results suggest that H_2S donor treatment can inhibit M1 and M2 macrophage infiltration in UUO mice.

3.4. NLRP3 inflammasome activation contributes to M1 and M2 macrophage infiltration, tissue damage and fibrosis in the obstructed kidneys of UUO mice

NF-κB and IL-4/STAT6 signaling pathways have been demonstrated to have a significant role in mediating the process of M1 and M2 macrophage polarization, respectively [34,35]. We found that levels of phosphorylated NF-κB p65 subunit, phosphorylated STAT6, as well as IL-4 protein in kidneys were increased from day 3 to day 14 after UUO compared with the sham group (Fig. 5A, B and C), indicating the activation of NF-κB and IL-4/STAT6 signaling pathways in obstructed kidneys of UUO mice. The crosstalk between NLRP3 inflammasome and NF-κB pathway has been widely investigated [12,36]. More recently,
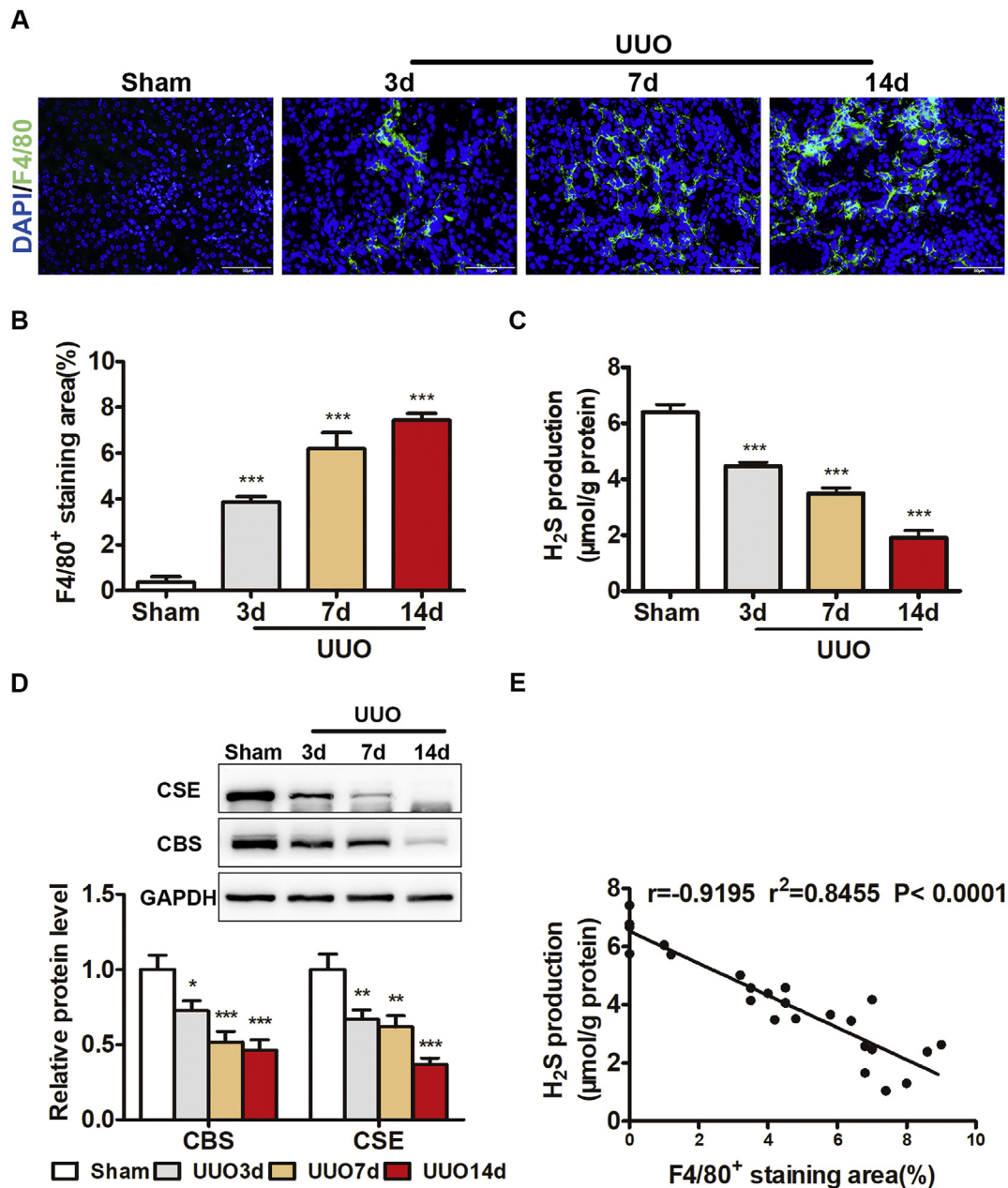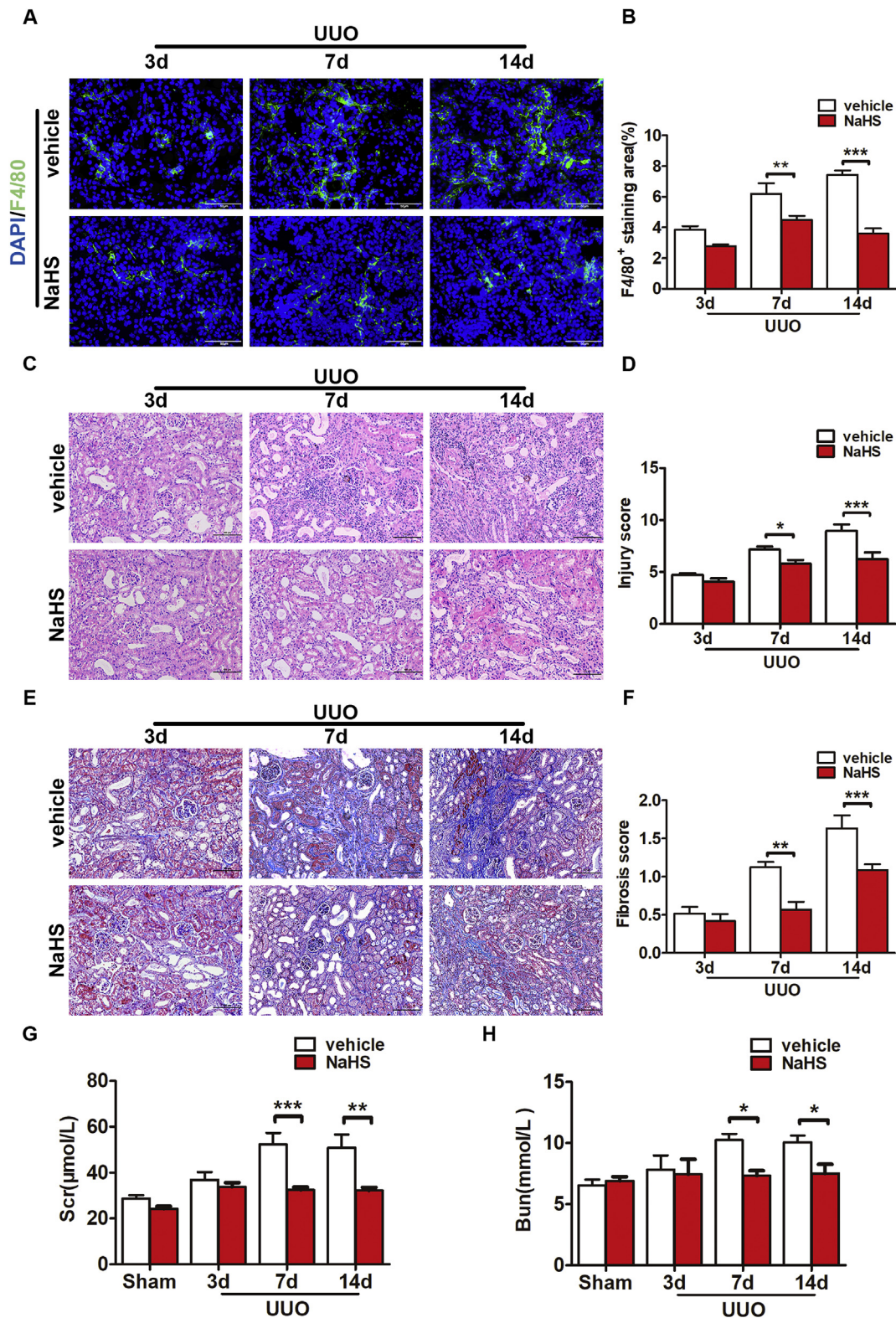
Fig. 1. Downregulation of H_2S production is associated with increased macrophage infiltration in obstructed kidneys of UUO mice. Mice were subjected to UUO. Renal tissues were harvested at the indicated time points. Mice that received the Sham operation served as controls. A, F4/80 immunofluorescent staining of renal tissues. Scale bar = 50 μm. B, Quantitative analysis for F4/80 positive staining. C, H_2S production in renal tissues. D, Protein levels of CBS and CSE in renal tissues. Representative protein bands were presented on the top of the histograms. E, Correlation analysis between H_2S content and F4/80 positive staining area in the kidney. Data were expressed as mean ± SEM (n = 6). *p < 0.05, **p < 0.01, ***p < 0.001 compared to the Sham group.

Liu et al. report that NLRP3 regulates macrophage M2 polarization through the up-regulation of IL-4 in asthma [9]. We found that UUO-induced activation of NF-κB and IL-4/STAT6 pathways was accompanied by NLRP3 inflammasome activation, as evidenced by increased levels of NLRP3 and cleaved caspase-1 p10 fragments. In addition, specific NLRP3 inhibitor, 16673-34-0, significantly reduced the levels of phosphorylated NF-κB p65 subunit, phosphorylated STAT6 (Fig. 5D and E), as well as IL-4 protein (Fig. 5F) in obstructed kidneys of UUO mice, suggesting that NLRP3 acts upstream of NF-κB and IL-4/STAT6 signaling pathways.

As shown in Fig. 6A-D, double immunofluorescence staining showed that the percentages of both iNOS$^+$/F4/80$^+$ cells and CD206$^+$/F4/80$^+$ cells in total F4/80$^+$ cells were significantly lower in obstructed kidneys of NLRP3 inhibitor-treated UUO mice as compared with saline-

treated UUO mice. Administration of NLRP3 inhibitor also significantly reduced the mRNA levels of M1 markers (Rantes, TNFα, IL-1β and IL-6) and M2 markers (CD206, Arg-1, and TIMP-1) in obstructed kidneys of UUO mice (Fig. 6E and F).

We also observed the effect of NLRP3 inhibitor on UUO-induced renal damage and fibrosis. It was found that obstructed kidneys of NLRP3 inhibitor-treated UUO mice exhibited less structural alteration when compared to saline-treated UUO mice as evidenced by reduced tubular dilation, infiltrating inflammatory cells and basement membrane thickening (Fig. 7A). The renal tubulointerstitial injury scores were reduced to 5.8 after the administration of NLRP3 inhibitor (Fig. 7B). Masson's trichrome staining indicated that the extensive deposition of fibrillar collagen and the destruction of normal renal architecture observed in obstructed kidneys of UUO mice were markedly
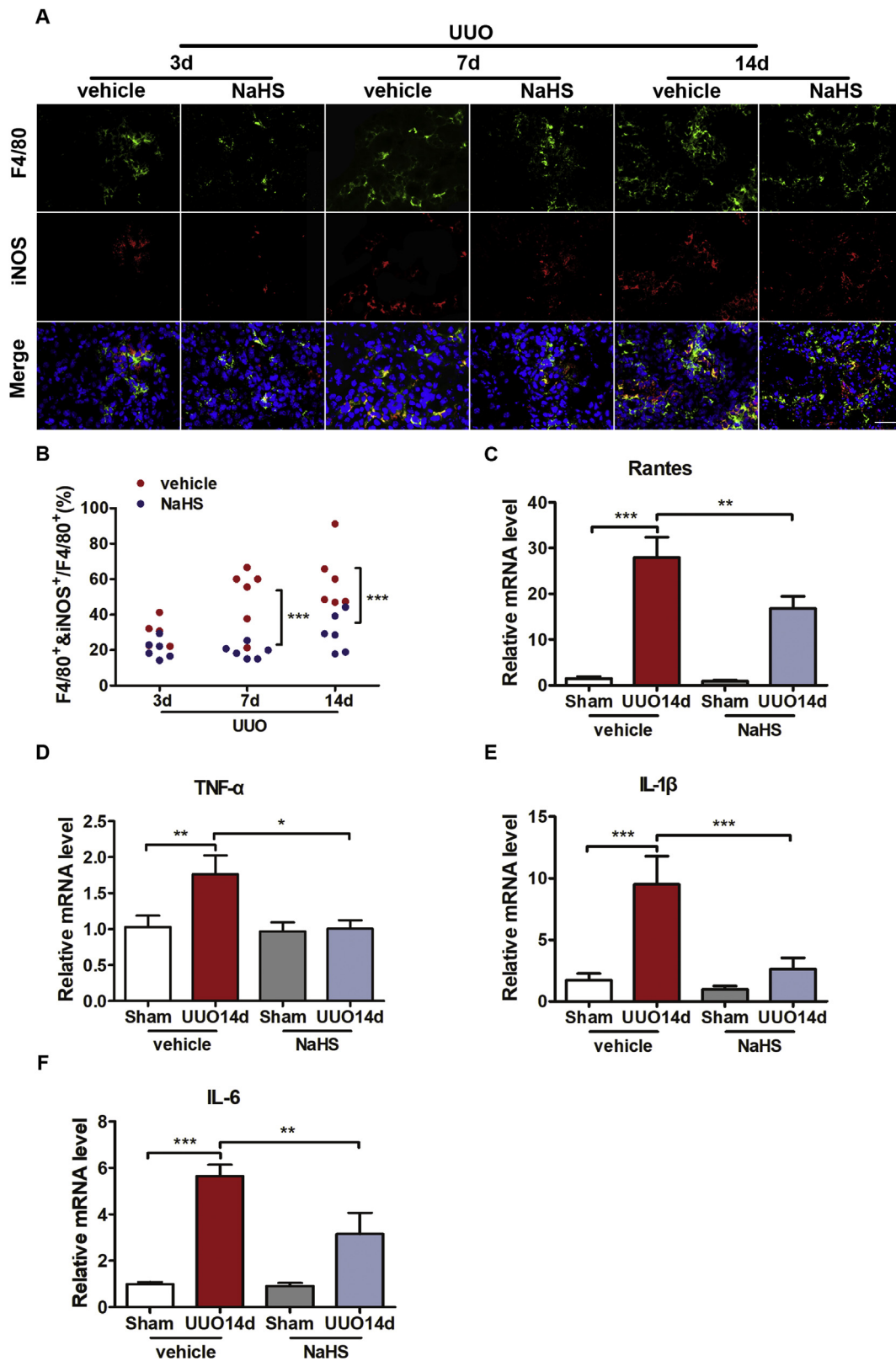
Fig. 2. H$_2$S donor attenuates macrophage infiltration, tissue damage and fibrosis in obstructed kidneys of UUO mice. Mice were subjected to UUO and treated with saline or NaHS (50 μg/kg/d, ip). Renal tissues were harvested at the indicated time points. Mice that received the Sham operation served as controls. A, F4/80 immunofluorescent staining of renal tissues. Scale bar = 20 μm. B. Quantitative analysis for F4/80 positive staining. C, Hematoxylin and eosin staining of renal tissues. Scale bar = 100 μm. D, The tubulointerstitial injury score. E, Masson's trichrome staining of renal tissues. Scale bar = 100 μm. F, The tubulointerstitial fibrosis score. G, Serum creatinine (Scr). H, Blood urea nitrogen (Bun). Data were expressed as mean ± SEM, n = 6, *p < 0.05, **p < 0.01, ***p < 0.001.

attenuated by NLRP3 inhibitor (Fig. 7C and D). UUO mice receiving NLRP3 inhibitor also showed a significant decrease in Scr and Bun concentrations at 7 days after the injection of NLRP3 inhibitor as compared with saline-treated UUO mice (Fig. 7E and F).

Taken together, these findings suggest that blockade of NLRP3 in-flammasome suppresses M1 and M2 macrophage infiltration by

Fig. 3. H$_2$S donor inhibits M1 macrophage infiltration in obstructed kidneys of UUO mice. A and B, Mice were subjected to UUO and treated with saline or NaHS (50 µg/kg/d, ip). Renal tissues were harvested at the indicated time points. A, M1 macrophages were shown via double immunofluorescent staining of F4/80 (green) and M1 marker iNOS (red). Nuclei were counterstained with 4′,6-diamidino-2-phenylindole (DAPI) (blue). Merge image represented the staining of F4/80$^+$ and iNOS$^+$ cells in renal tissues. Scale bar = 20 µm. B, The proportion of iNOS$^+$/F4/80$^+$ cells in total F4/80$^+$ cells. C–F, Sham and UUO mice were treated with saline or NaHS (50 µg/kg/d, ip). Two weeks later, renal tissues were harvested to examine the relative mRNA expression of M1 markers Rantes (C), TNF-α (D), IL-1β (E), and IL-6 (F). Data were expressed as mean ± SEM, n = 6, *p < 0.05, **p < 0.01, ***p < 0.001. (For interpretation of the references to colour in this figure legend, the reader is referred to the Web version of this article.)
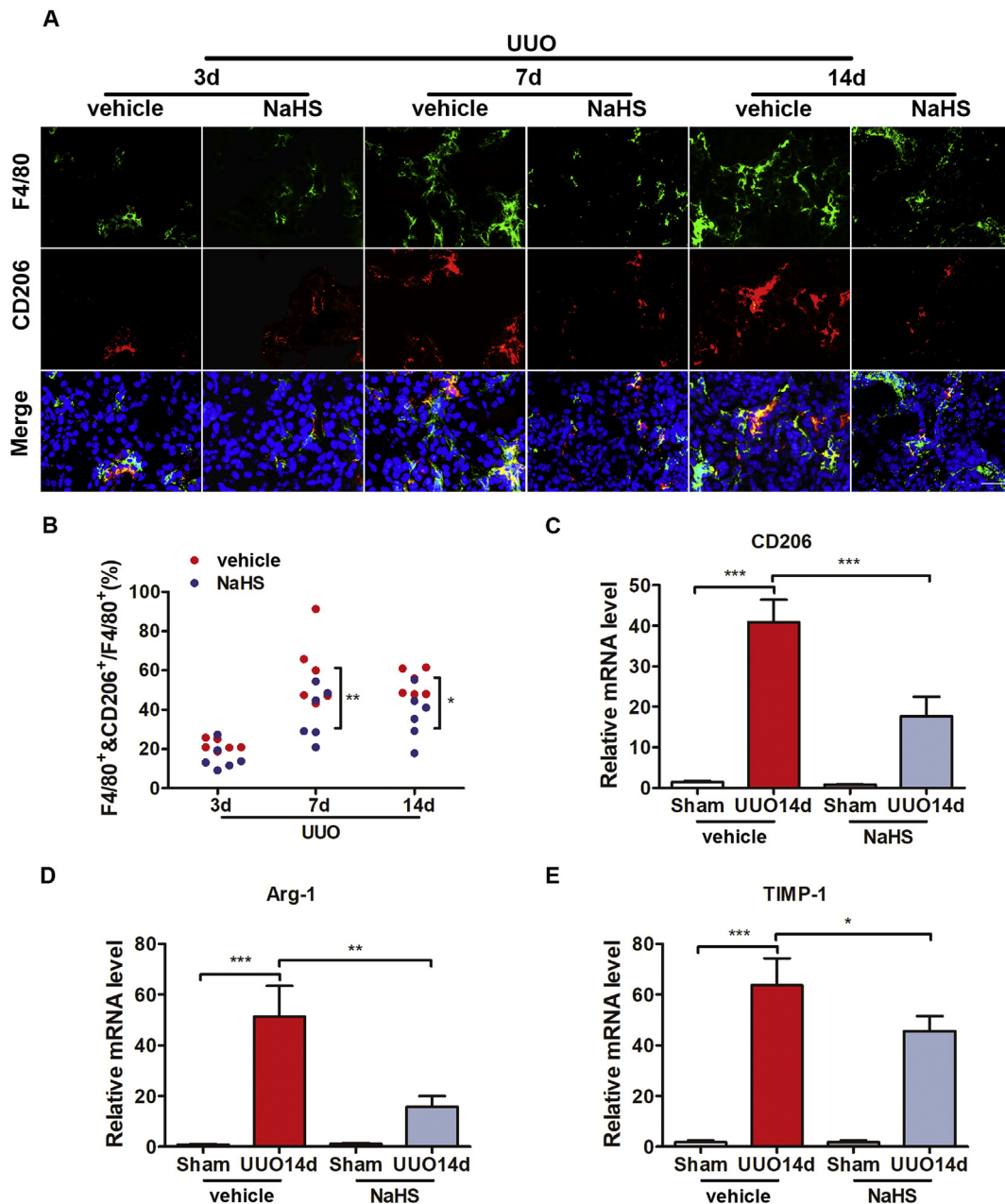
Fig. 4. H$_2$S donor inhibits M2 macrophage infiltration in obstructed kidneys of UUO mice. A and B, Mice were subjected to UUO and treated with saline or NaHS (50 μg/kg/d, ip). Renal tissues were harvested at the indicated time points. A, M2 macrophages were shown via double immunofluorescent staining of F4/80 (green) and M2 marker CD206 (red). Nuclei were counterstained with DAPI (blue). Merge image represented the staining of F4/80$^+$ and CD206$^+$ cells in renal tissues. Scale bar = 20 μm. B, The proportion of CD206$^+$/F4/80$^+$ cells in total F4/80$^+$ cells. C–F, Sham and UUO mice were treated with saline or NaHS (50 μg/kg/ d, ip). Two weeks later, renal tissues were harvested to examine the relative mRNA expression of M2 markers CD206 (C), Arg-1 (D), and TIMP-1 (E). Data were expressed as mean ± SEM, n = 6, *p < 0.05, **p < 0.01, ***p < 0.001. (For interpretation of the references to colour in this figure legend, the reader is referred to the Web version of this article.)

inactivates NF-κB and IL-4/STAT6 signaling pathways, thus preventing tissue damage and fibrosis in obstructed kidneys of UUO mice.

3.5. H$_2$S donor suppresses the activation of NLRP3 inflammasome, NF-κB and IL-4/STAT6 signaling pathways in the obstructed kidneys of UUO mice

As shown in Fig. 8A, NaHS treatment at a dose of 50 μg/kg/d for 14 days significantly reduced protein levels of NLRP3 and cleaved caspase-1 p10 fragments in obstructed kidneys of UUO mice. In addition, phosphorylation of NF-κB p65 subunit and STAT6, as well as IL-4 protein levels in obstructed kidneys of UUO mice were also reduced by NaHS treatment (Fig. 8B and C). Taken together, these findings suggest

that NaHS can inhibit the activation of NLRP3 inflammasome, NF-κB and IL-4/STAT6 signaling pathways in obstructed kidneys of UUO mice.

4. Discussion

Dysregulation of endogenous H$_2$S production has been reported during the development of CKD [20–23]. Clinically, it has been found that plasma H$_2$S levels are significantly decreased in non-dialysis CKD and hemodialysis patients, as well as patients with sepsis-associated acute kidney injury, compared to healthy controls [37,38]. Furthermore, there is a significant inverse correlation between the plasma levels of H$_2$S and creatinine or urea nitrogen in SA-AKI patients [37]. In

Y. Zhou, et al.
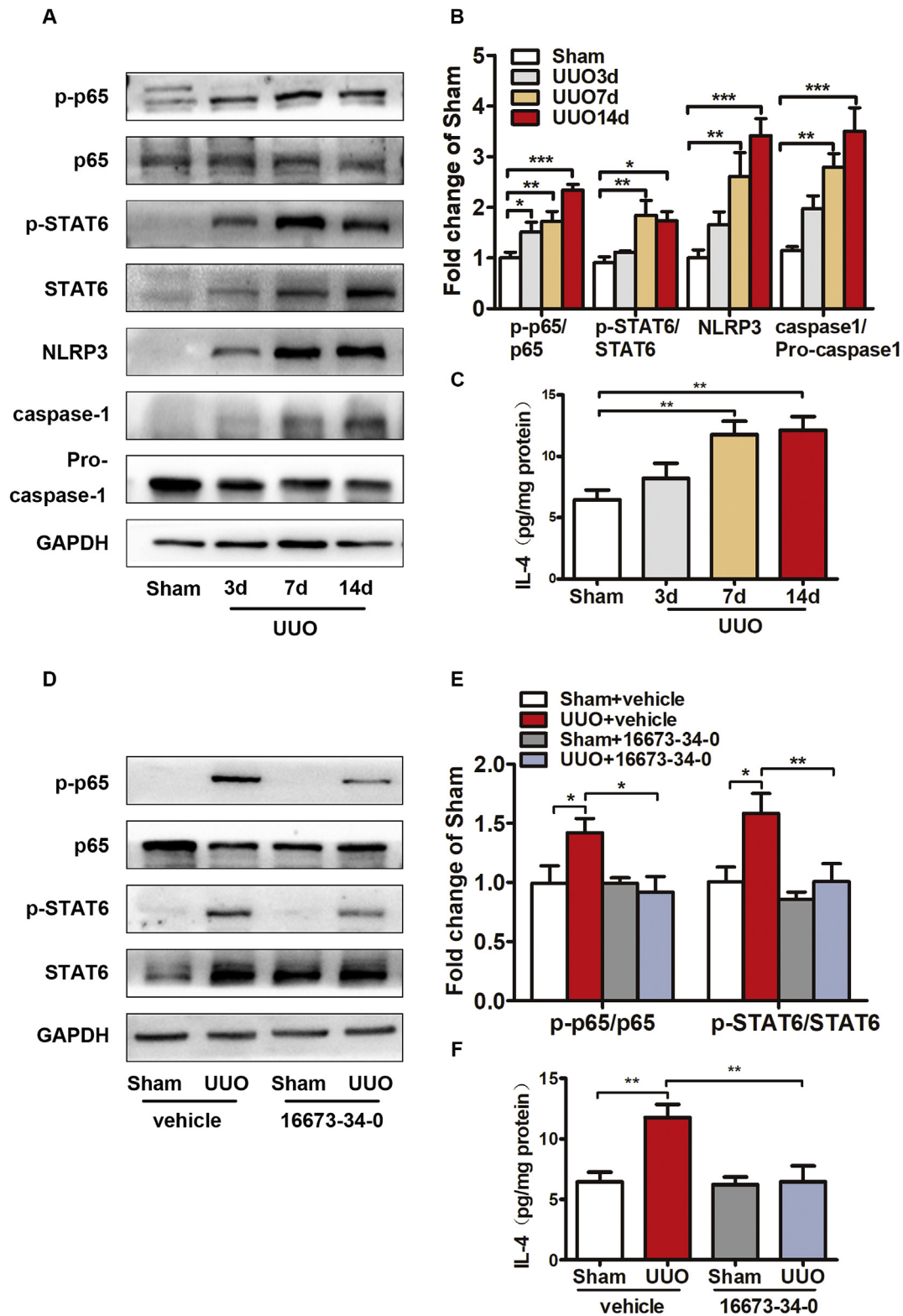
Fig. 5. NLRP3 acts upstream of NF-κB and IL-4/STAT6 signaling pathways in obstructed kidneys of UUO. A-C, Mice were subjected to UUO. Renal tissues were harvested at the indicated time points. Mice that received the Sham operation served as controls. A and B, Protein levels of phosphorylated NF-κB p65 subunit (p-p65), p65, phosphorylated STAT6 (p-STAT6), STAT6, NLRP3, cleaved caspase-1, Pro-caspase-1 and GAPDH in renal tissues. Representative protein bands (A) were presented on the left of the histograms (B). C, Protein levels of IL-4 in renal tissues were detected by using ELISA assay. D-F, Sham and UUO mice were treated with vehicle or specific NLRP3 inhibitor 16673-34-0 (10 mg/kg/d, ip). Renal tissues were harvested 7 days later. D and E, Protein levels of p-p65, p65, p-STAT6, STAT6, and GAPDH in renal tissues. Representative protein bands (D) were presented on the left of the histograms (E). F, Protein levels of IL-4 in renal tissues. Data were expressed as mean ± SEM, n = 6, *$p < 0.05$, **$p < 0.01$, ***$p < 0.001$.
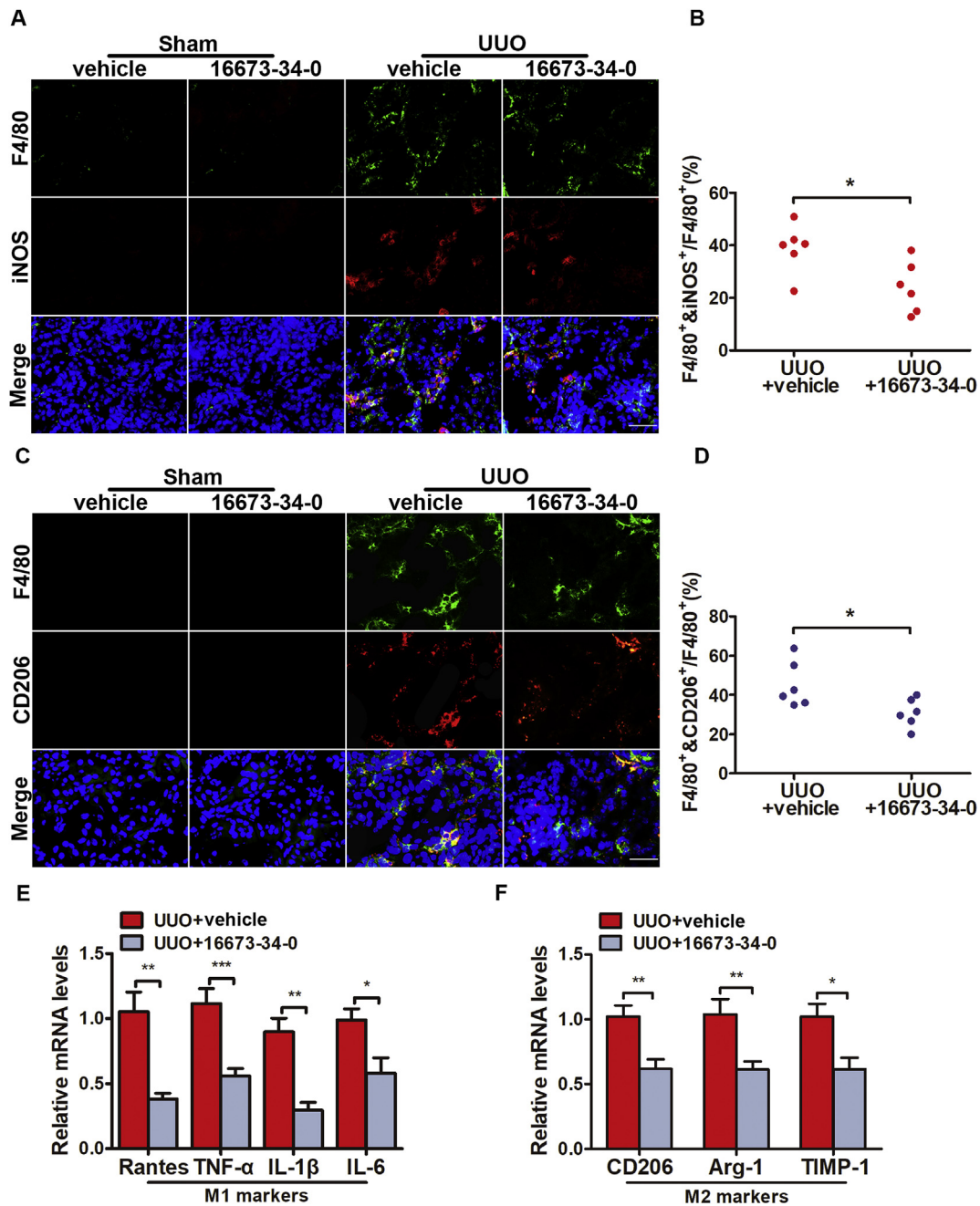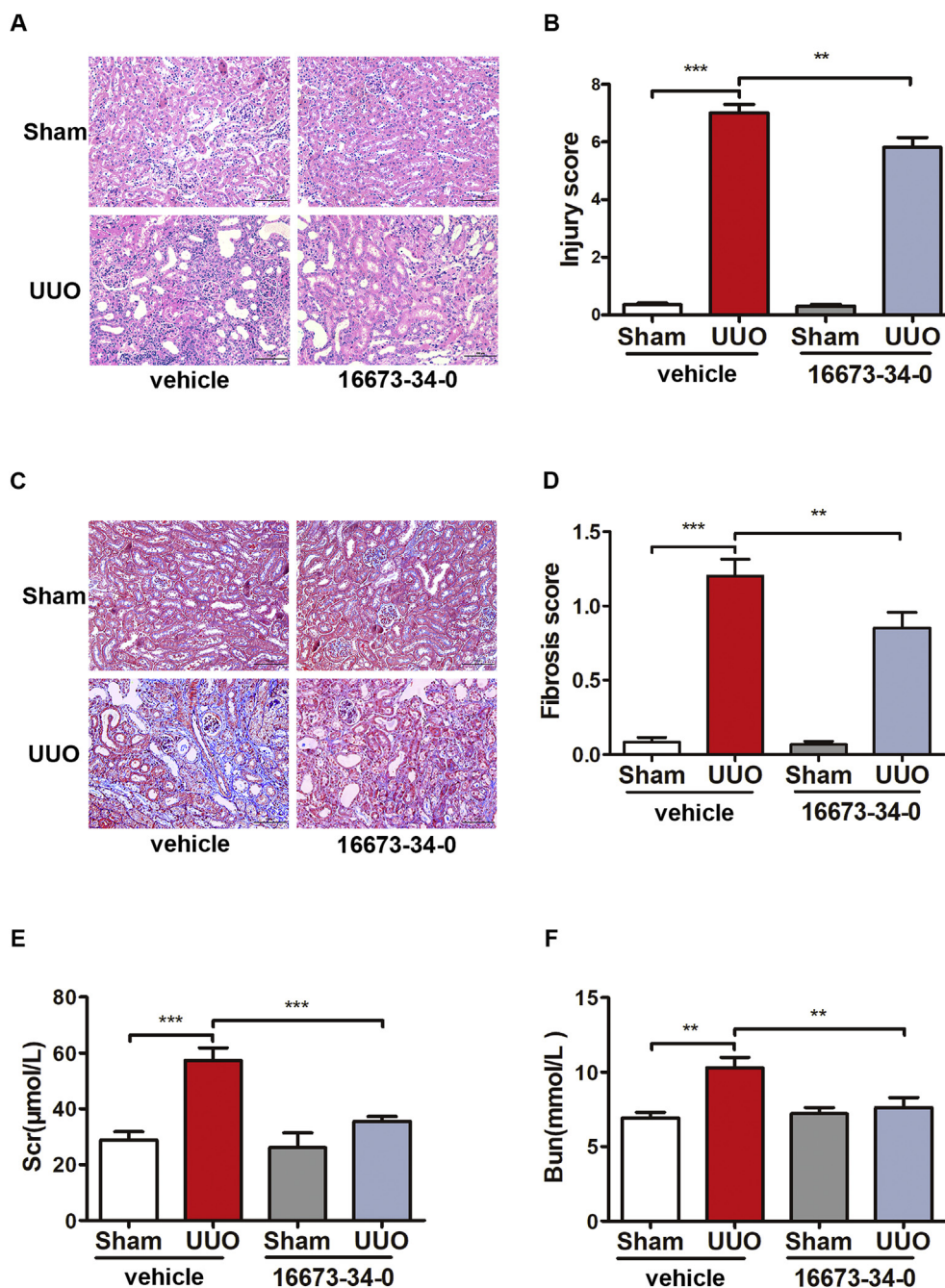
Fig. 6. NLRP3 inhibitor reduces M1 and M2 macrophage infiltration in obstructed kidneys of UUO. Sham and UUO mice were treated with the vehicle or specific NLRP3 inhibitor 16673-34-0 (10 mg/kg/d, ip). Renal tissues were harvested 7 days later. A, M1 macrophages were shown via double immunofluorescent staining of F4/80 (green) and M1 marker iNOS (red). Nuclei were counterstained with DAPI (blue). Merge image represented the staining of $F4/80^+$ and $iNOS^+$ cells in renal tissues. Scale bar = 20 μm. B, The proportion of $iNOS^+/F4/80^+$ cells in total $F4/80^+$ cells. C, M2 macrophages were shown via double immunofluorescent staining of F4/80 (green) and M2 marker CD206 (red). Nuclei were counterstained with DAPI (blue). Merge image represented the staining of $F4/80^+$ and $CD206^+$ cells in renal tissues. Scale bar = 20 μm. D, The proportion of $CD206^+/F4/80^+$ cells in total $F4/80^+$ cells. E, The relative mRNA expression of M1 markers Rantes, TNF-α, IL-1β, and IL-6. F, The relative mRNA expression of M2 markers CD206, Arg-1, and TIMP-1. Data were expressed as mean ± SEM, n = 6, *p < 0.05, **p < 0.01, ***p < 0.001. (For interpretation of the references to colour in this figure legend, the reader is referred to the Web version of this article.)

animal models, decreased plasma and/or renal H_2S contents have been shown in CKD induced by UUO [22], 5/6 nephrectomy [23], or diabetes [39]. In contrast, Song et al. demonstrate that renal CSE expression is gradually upregulated from 3 days to 14 days after UUO [40]. Despite these inconsistent data on the responsiveness of endogenous H_2S pathway to CKD, NaHS treatment has been shown to attenuate renal damages in CKD models induced by both UUO and diabetes [19,39], which is in agreement with the present study. Nevertheless, our findings provide evidence that decreases of renal CBS/CSE protein

expression and H_2S production occur from 3 days to 14 days after ureteral ligation and even contribute to the pathogenesis of UUO-induced renal injury and fibrosis.

Macrophage recruitment plays an essential role during the injury and repair phases after an obstructive injury in the kidney. In the early phase following ureteral obstruction, M1 macrophages promote inflammation and amplify injury through the release of proinflammatory cytokines. In the late phase after UUO, macrophages undergo a switch from a pro-inflammatory M1 phenotype to a trophic M2 phenotype that

Fig. 7. NLRP3 inhibitor alleviates tissue damage and fibrosis in obstructed kidneys of UUO mice. Sham and UUO mice were treated with the vehicle or specific NLRP3 inhibitor 16673-34-0 (10 mg/kg/d, ip). Renal tissues were harvested 7 days later. A, Hematoxylin and eosin staining of renal tissues. Scale bar = 100 μm. B, The tubulointerstitial injury score. C, Masson's trichrome staining of renal tissues. Scale bar = 100 μm. D, The tubulointerstitial fibrosis score. E, Serum creatinine (Scr). F, Blood urea nitrogen (Bun). Data were expressed as mean ± SEM, n = 6, **p < 0.01, ***p < 0.001.

plays an important role in the repair process acting as scavengers of cell debris and promoting regeneration [5,41]. Many studies have confirmed the direct effect of H_2S on macrophages in vivo or in vitro. For instance, H_2S can reduce the level of oxidative stress of macrophages stimulated by LPS [42] or ox-LDL [25]; a novel slow-releasing hydrogen sulfide donor exerts anti-inflammatory effects by reducing the levels of inflammatory factors secreted by macrophages [43]; furthermore, H_2S can even inhibit the inflammatory response through epigenetic modification [44] or regulation of calcium ion [45] in mouse RAW264.7 macrophages. However, the impact of H_2S on M2 macrophage polarization is only observed in some acute injury models. For example, H_2S donors have been demonstrated to promote M2 polarization of

macrophages and microglia in murine models of myocardial infarction and LPS-induced neuroinflammation, respectively [46,47]. Notably, Cao et al. have reported that H_2S donor significantly inhibits bleomycin-induced production of IL-4, the key cytokine in both Th2 lymphocyte polarization and M2 macrophage polarization, therefore exerting a protective efficacy against bleomycin-induced pulmonary fibrosis by regulating Th1/Th2 balance [48]. Moreover, JAK/STAT6, a critical signaling pathway in M2 macrophage polarization, is also downregulated by H_2S donor NaHS in a rat model of diabetes-associated myocardial fibrosis [49]. In line with these findings, our results demonstrated that NaHS treatment led to a significant decrease in IL-4 expression and STAT6 phosphorylation, which might contribute to the
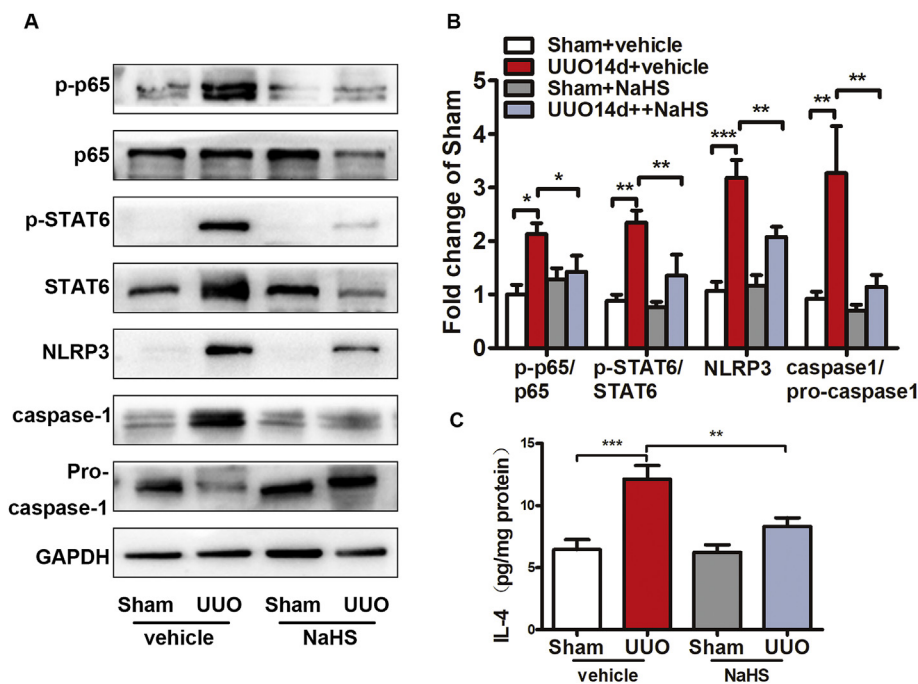
Fig. 8. H$_2$S donor inhibits the activation of NLRP3 inflammasome, NF-κB and IL-4/STAT6 signaling pathways in obstructed kidneys of UUO mice. Sham and UUO mice were treated with saline or NaHS (50 μg/kg/d, ip). Renal tissues were harvested 14 days later. A and B, Protein levels of p-p65, p65, p-STAT6, STAT6, NLRP3, cleaved caspase-1, Pro-caspase-1 and GAPDH in renal tissues. Representative protein bands (A) were presented on the left of the histograms (B). C, Protein levels of IL-4 in renal tissues. Data were expressed as mean ± SEM, n = 6, *p < 0.05, **p < 0.01, ***p < 0.001.

inhibitory effect of NaHS on M2 macrophage infiltration in the obstructed kidney.

Activation of NF-κB and IL-4/STAT6 signaling pathways has been implicated in the polarization of M1 and M2 macrophage phenotypes, respectively [34,35]. In the context of renal injury, NF-κB activation is characteristic of M1 macrophages and promotes renal injury in crescentic glomerulonephritis [50]. Macrophages in which NF-κB activation is inhibited acquire an anti-inflammatory phenotype and suppress renal injury following adoptive transfer it in a rat model of nephrotoxic nephritis [51]. On the other hand, mice lacking the IL-4 receptor α-chain are protected from renal fibrosis induced by UUO and folic acid, concomitant with reduced STAT6 signaling in the kidney and reduced numbers of M2 macrophages [52]. Furthermore, STAT6 deletion in the bone marrow compartment was sufficient to reduce renal fibrosis markedly in the obstructed kidney [53]. In line with these findings, this study found that UUO-induced M1 and M2 macrophage infiltration in the kidney was accompanied by activation of NF-κB and IL-4/STAT6 signaling pathways. In addition, both H$_2$S donor and NLRP3 inhibitor inactivated NF-κB and IL-4/STAT6, thus resulting in a significant reduction of M1 and M2 macrophage infiltration. Taken together, these results emphasize the central role of NF-κB and IL-4/STAT6 signaling pathways in M1 and M2 macrophage-mediated kidney damage.

NLRP3 inflammasome has been shown to contribute to the pathogenesis of various kidney diseases [16,17,54,55]. However, whether NLRP3 activation contributes to the increased infiltration of M1 and M2 macrophages in CKD remains largely unknown. Previous studies indicate that NLRP3 can mediate NF-κB activation [12,13], and meanwhile transactivate IL-4 promoter to increase IL-4 expression in peripheral blood monocyte-derived macrophages [9]. In this study, we provided the first in vivo evidence that blockade of NLRP3 inflammasome inactivated NF-κB and IL-4/STAT6 signaling pathways, meanwhile attenuated M1 and M2 macrophage infiltration, renal injury and fibrosis in obstructed kidneys of UUO mice. These findings suggest that NLRP3 inflammasome activation may act upstream of NF-κB and IL-4/STAT6 signaling pathways to regulate M1/M2 macrophage infiltration, thus contributing to tissue damage and fibrosis in UUO-induced CKD.

H$_2$S has been reported to exert antioxidant, anti-apoptotic and anti-inflammatory actions to protect against renal injury and/or fibrosis induced by UUO [19,22,56], ischemia/reperfusion [57,58], adenine [59], and high-fat diet [60]. However, the signal transduction

mechanisms responsible for the renal protective effects of H$_2$S remain largely unknown. H$_2$S has been shown to attenuate renal fibrosis by inhibiting TGF-β/Smad and ROS-AMPK pathways [19,56], or by activating Nrf2 antioxidant pathway [20]. As discussed above, NLRP3-dependent activation of NF-κB and IL4/STAT6 signaling pathways may contribute to the M1 and M2 macrophage infiltration in obstructed kidneys of UUO mice. Previous in vitro studies have reported that H$_2$S blocks the activation of NLRP3 and NF-κB in macrophages exposed to various stimuli such as LPS and oxidative stress [24,43]. H$_2$S can also decrease the production of IL-4 in bronchoalveolar lavage fluid of bleomycin-induced pulmonary fibrosis model [48]. In this study, we provided the in vivo evidence that H$_2$S treatment alleviated UUO-induced NLRP3 inflammasome activation, NF-κB p65 subunit/STAT6 phosphorylation, IL-4 production, and M1/M2 macrophage infiltration in the obstructed kidney tissues. Taken together, these findings suggest that inhibition of NLRP3 and the downstream NF-κB and IL4/STAT6 signaling pathways as well as M1 and M2 macrophage infiltration may contribute to the protection against UUO-induced renal injury and fibrosis afforded by H$_2$S.

5. Conclusion

Our results have indicated that the increased number of infiltrating macrophages in the obstructed renal interstitial is associated with decreased H$_2$S content in the renal tissue. The therapeutic effects of H$_2$S on UUO-induced renal injury and fibrosis are at least in part by inhibition of M1 and M2 macrophage infiltration. H$_2$S can suppress NLRP3 activation and subsequently inactivates NF-κB and IL4/STAT6 signaling, which may contribute to the anti-inflammatory and anti-fibrotic effects of H$_2$S.

Authour contribution

Yueyuan Zhou:Methodology, Investigation, Writing - Original Draft, Visualization. Xiaoyan Zhu : Conceptualization, Writing - Review & Editing, Visualization. Xuan Wang:Formal analysis, Visualization. Yi Peng:Methodology. Jiankui Du:Software, Formal analysis. Hongling Yin: Methodology. Hui Yang:Methodology. Xin Ni:Conceptualization, Resources, Writing - Review & Editing, Supervision, Project administration. Weiru Zhang: Conceptualization, Resources, Writing - Review &

Editing, Supervision, Funding acquisition.

Declaration of competing interest

No conflicts of interest, financial or otherwise, are declared by the authors.

Acknowledgments

Appendix A. Supplementary data

Supplementary data to this article can be found online at https://doi.org/10.1016/j.yexcr.2019.111779.

References

[1] A. Khwaja, M. El Kossi, J. Floege, M. El Nahas, The management of CKD: a look into the future, Kidney Int. 72 (11) (2007) 1316–1323.

[2] Y. Liu, Cellular and molecular mechanisms of renal fibrosis, Nat. Rev. Nephrol. 7 (12) (2011) 684–696.

[3] P.M. Tang, D.J. Nikolic-Paterson, H.Y. Lan, Macrophages: versatile players in renal inflammation and fibrosis, Nat. Rev. Nephrol. 15 (3) (2019) 144–158.

[4] F.O. Martinez, L. Helming, S. Gordon, Alternative activation of macrophages: an immunologic functional perspective, Annu. Rev. Immunol. 27 (2009) 451–483.

[5] T.A. Wynn, K.M. Vannella, Macrophages in tissue repair, regeneration, and fibrosis, Immunity 44 (3) (2016) 450–462.

[6] S. Chakarov, H.Y. Lim, L. Tan, et al., Two distinct interstitial macrophage populations coexist across tissues in specific subtissular niches, Science 363 (6432) (2019).

[7] M. Huang, Y. Li, K. Wu, et al., Paraquat modulates microglia M1/M2 polarization via activation of TLR4-mediated NF-kappaB signaling pathway, Chem. Biol. Interact. 310 (2019) 108743.

[8] J. Slusarczyk, E. Trojan, K. Glombik, et al., Targeting the NLRP3 inflammasome-related pathways via tianeptine treatment-suppressed microglia polarization to the M1 phenotype in lipopolysaccharide-stimulated cultures, Int. J. Mol. Sci. 19 (7) (2018).

[9] Y. Liu, X. Gao, Y. Miao, et al., NLRP3 regulates macrophage M2 polarization through up-regulation of IL-4 in asthma, Biochem. J. 475 (12) (2018) 1995–2008.

[10] D. Carneros, E.M. Santamaria, E. Larequi, et al., Cardiotrophin-1 is an anti-inflammatory cytokine and promotes IL-4-induced M2 macrophage polarization, FASEB J. 33 (6) (2019) 7578–7587.

[11] E. Latz, T.S. Xiao, A. Stutz, Activation and regulation of the inflammasomes, Nat. Rev. Immunol. 13 (6) (2013) 397–411.

[12] S.A. Conos, K.W. Chen, D. De Nardo, et al., Active MLKL triggers the NLRP3 inflammasome in a cell-intrinsic manner, Proc. Natl. Acad. Sci. U.S.A. 114 (6) (2017) E961–E969.

[13] L. Zhang, Y. Fan, H. Su, et al., Chlorogenic acid methyl ester exerts strong anti-inflammatory effects via inhibiting the COX-2/NLRP3/NF-kappaB pathway, Food Funct. 9 (12) (2018) 6155–6164.

[14] W. Liu, X. Zhang, M. Zhao, et al., Activation in M1 but not M2 macrophages contributes to cardiac remodeling after myocardial infarction in rats: a critical role of the calcium sensing receptor/NRLP3 inflammasome, Cell. Physiol. Biochem. 35 (6) (2015) 2483–2500.

[15] M. Bruchard, C. Rebe, V. Derangere, et al., The receptor NLRP3 is a transcriptional regulator of TH2 differentiation, Nat. Immunol. 16 (8) (2015) 859–870.

[16] A. Vilaysane, J. Chun, M.E. Seamone, et al., The NLRP3 inflammasome promotes renal inflammation and contributes to CKD, J. Am. Soc. Nephrol. : JASN (J. Am. Soc. Nephrol.) 21 (10) (2010) 1732–1744.

[17] H.J. Anders, B. Suarez-Alvarez, M. Grigorescu, et al., The macrophage phenotype and inflammasome component NLRP3 contributes to nephrocalcinosis-related chronic kidney disease independent from IL-1-mediated tissue injury, Kidney Int. 93 (3) (2018) 656–669.

[18] C.Q. Chen, H. Xin, Y.Z. Zhu, Hydrogen sulfide: third gaseous transmitter, but with great pharmacological potential, Acta Pharmacol. Sin. 28 (11) (2007) 1709–1716.

[19] K.J. Jung, H.S. Jang, J.I. Kim, S.J. Han, J.W. Park, K.M. Park, Involvement of hydrogen sulfide and homocysteine transsulfuration pathway in the progression of kidney fibrosis after ureteral obstruction, Biochim. Biophys. Acta 1832 (12) (2013) 1989–1997.

[20] J. Zheng, T. Zhao, Y. Yuan, N. Hu, X. Tang, Hydrogen sulfide (H2S) attenuates uranium-induced acute nephrotoxicity through oxidative stress and inflammatory response via Nrf2-NF-kappaB pathways, Chem. Biol. Interact. 242 (2015) 353–362.

[21] L. Marko, I.A. Szijarto, M.R. Filipovic, et al., Role of cystathionine gamma-lyase in immediate renal impairment and inflammatory response in acute ischemic kidney injury, Sci. Rep. 6 (2016) 27517.

[22] S.J. Han, M.R. Noh, J.M. Jung, et al., Hydrogen sulfide-producing cystathionine gamma-lyase is critical in the progression of kidney fibrosis, Free Radic. Biol. Med. 112 (2017) 423–432.

[23] M.A. Aminzadeh, N.D. Vaziri, Downregulation of the renal and hepatic hydrogen sulfide (H2S)-producing enzymes and capacity in chronic kidney disease, Nephrol. Dial. Transplant. 27 (2) (2012) 498–504 official publication of the European Dialysis and Transplant Association - European Renal Association.

[24] Z. Lin, N. Altaf, C. Li, et al., Hydrogen sulfide attenuates oxidative stress-induced NLRP3 inflammasome activation via S-sulfhydrating c-Jun at Cys269 in macrophages, Biochim. Biophys. Acta (BBA) - Mol. Basis Dis. 1864 (9 Pt B) (2018) 2890–2900.

[25] J. Du, Y. Huang, H. Yan, et al., Hydrogen sulfide suppresses oxidized low-density lipoprotein (ox-LDL)-stimulated monocyte chemoattractant protein 1 generation from macrophages via the nuclear factor kappaB (NF-kappaB) pathway, J. Biol. Chem. 289 (14) (2014) 9741–9753.

[26] J. Ji, P. Xiang, T. Li, et al., NOSH-NBP, a novel nitric oxide and hydrogen sulfide-releasing hybrid, attenuates ischemic stroke-induced neuroinflammatory injury by modulating microglia polarization, Front. Cell. Neurosci. 11 (2017) 154.

[27] J. Barrera-Chimal, G.R. Estrela, S.M. Lechner, et al., The myeloid mineralocorticoid receptor controls inflammatory and fibrotic responses after renal injury via macrophage interleukin-4 receptor signaling, Kidney Int. 93 (6) (2018) 1344–1355.

[28] D. Wang, M. Xiong, C. Chen, et al., Legumain, an asparaginyl endopeptidase, mediates the effect of M2 macrophages on attenuating renal interstitial fibrosis in obstructive nephropathy, Kidney Int. 94 (1) (2018) 91–101.

[29] Y. Kusunoki, I. Matsui, T. Hamano, et al., Excess 25-hydroxyvitamin D3 exacerbates tubulointerstitial injury in mice by modulating macrophage phenotype, Kidney Int. 88 (5) (2015) 1013–1029.

[30] R.L. Chevalier, M.S. Forbes, B.A. Thornhill, Ureteral obstruction as a model of renal interstitial fibrosis and obstructive nephropathy, Kidney Int. 75 (11) (2009) 1145–1152.

[31] C. Marchetti, J. Chojnacki, S. Toldo, et al., A novel pharmacologic inhibitor of the NLRP3 inflammasome limits myocardial injury after ischemia-reperfusion in the mouse, J. Cardiovasc. Pharmacol. 63 (4) (2014) 316–322.

[32] S.F. Du, X.L. Wang, C.L. Ye, et al., Exercise training ameliorates bleomycin-induced epithelial mesenchymal transition and lung fibrosis through restoration of H2 S synthesis, Acta Physiol. 225 (2) (2019) e13177.

[33] B.X. Li, Y.T. Tang, W. Wang, et al., Fluorofenidone attenuates renal interstitial fibrosis in the rat model of obstructive nephropathy, Mol. Cell. Biochem. 354 (1–2) (2011) 263–273.

[34] F. Furuya, T. Ishii, S. Tamura, et al., The ligand-bound thyroid hormone receptor in macrophages ameliorates kidney injury via inhibition of nuclear factor-kappaB activities, Sci. Rep. 7 (2017) 43960.

[35] A. Vural, N.R. Nabar, I.Y. Hwang, et al., Galphai2 signaling regulates inflammasome priming and cytokine production by biasing macrophage phenotype determination, J. Immunol. 202 (5) (2019) 1510–1520.

[36] X. Wang, L. Jiang, L. Shi, et al., Zearalenone induces NLRP3-dependent pyroptosis via activation of NF-kappaB modulated by autophagy in INS-1 cells, Toxicology (2019) 152304.

[37] Y. Chen, S. Jin, X. Teng, et al., Hydrogen sulfide attenuates LPS-induced acute kidney injury by inhibiting inflammation and oxidative stress, Oxidative Med. Cell. Longev. 2018 (2018) 6717212.

[38] A.F. Perna, M.G. Luciano, D. Ingrosso, et al., Hydrogen sulphide-generating pathways in haemodialysis patients: a study on relevant metabolites and transcriptional regulation of genes encoding for key enzymes, Nephrol. Dial. Transplant. 24 (12) (2009) 3756–3763 official publication of the European Dialysis and Transplant Association - European Renal Association.

[39] X. Zhou, Y. Feng, Z. Zhan, J. Chen, Hydrogen sulfide alleviates diabetic nephropathy in a streptozotocin-induced diabetic rat model, J. Biol. Chem. 289 (42) (2014) 28827–28834.

[40] K. Song, F. Wang, Q. Li, et al., Hydrogen sulfide inhibits the renal fibrosis of obstructive nephropathy, Kidney Int. 85 (6) (2014) 1318–1329.

[41] S. Lee, S. Huen, H. Nishio, et al., Distinct macrophage phenotypes contribute to kidney injury and repair, J. Am. Soc. Nephrol. : JASN (J. Am. Soc. Nephrol.) 22 (2) (2011) 317–326.

[42] X.L. Wang, L.L. Pan, F. Long, et al., Endogenous hydrogen sulfide ameliorates NOX4 induced oxidative stress in LPS-stimulated macrophages and mice, Cell. Physiol. Biochem. : Int. J. Exp. Cell. Physiol. Biochem. pharmacol. 47 (2) (2018) 458–474.

[43] C.W. Huang, W. Feng, M.T. Peh, K. Peh, B.W. Dymock, P.K. Moore, A novel slow-releasing hydrogen sulfide donor, FW1256, exerts anti-inflammatory effects in mouse macrophages and in vivo, Pharmacol. Res. 113 (Pt A) (2016) 533–546.

[44] S. Liu, X. Wang, L. Pan, et al., Endogenous hydrogen sulfide regulates histone demethylase JMJD3-mediated inflammatory response in LPS-stimulated macrophages and in a mouse model of LPS-induced septic shock, Biochem. Pharmacol. 149 (2018) 153–162.

[45] G.V. Velmurugan, H. Huang, H. Sun, et al., Depletion of H2S during obesity enhances store-operated Ca2+ entry in adipose tissue macrophages to increase cytokine production, Sci. Signal. 8 (407) (2015) ra128.

[46] L. Miao, X. Shen, M. Whiteman, et al., Hydrogen sulfide mitigates myocardial infarction via promotion of mitochondrial biogenesis-dependent M2 polarization of macrophages, Antioxidants Redox Signal. 25 (5) (2016) 268–281.

[47] X. Zhou, Y. Cao, G. Ao, et al., CaMKKbeta-dependent activation of AMP-activated protein kinase is critical to suppressive effects of hydrogen sulfide on neuroinflammation, Antioxidants Redox Signal. 21 (12) (2014) 1741–1758.

[48] H. Cao, X. Zhou, J. Zhang, et al., Hydrogen sulfide protects against bleomycin-induced pulmonary fibrosis in rats by inhibiting NF-kappaB expression and regulating Th1/Th2 balance, Toxicol. Lett. 224 (3) (2014) 387–394.

[49] M. Liu, Y. Li, B. Liang, et al., Hydrogen sulfide attenuates myocardial fibrosis in diabetic rats through the JAK/STAT signaling pathway, Int. J. Mol. Med. 41 (4) (2018) 1867–1876.

[50] N. Tomita, R. Morishita, H.Y. Lan, et al., In vivo administration of a nuclear tran-scription factor-kappaB decoy suppresses experimental crescentic glomerulone-phritis, J. Am. Soc. Nephrol. : JASN (J. Am. Soc. Nephrol.) 11 (7) (2000) 1244–1252.

[51] H.M. Wilson, S. Chettibi, C. Jobin, D. Walbaum, A.J. Rees, D.C. Kluth, Inhibition of macrophage nuclear factor-κb leads to a dominant anti-inflammatory phenotype that attenuates glomerular inflammation in vivo, Am. J. Pathol. 167 (1) (2005) 27–37.

[52] H. Liang, Z. Zhang, J. Yan, et al., The IL-4 receptor α has a critical role in bone marrow–derived fibroblast activation and renal fibrosis, Kidney Int. 92 (6) (2017) 1433–1443.

[53] J. Yan, Z. Zhang, J. Yang, W.E. Mitch, Y. Wang, JAK3/STAT6 stimulates bone marrow-derived fibroblast activation in renal fibrosis, J. Am. Soc. Nephrol. : JASN (J. Am. Soc. Nephrol.) 26 (12) (2015) 3060–3071.

[54] H.H. Chi, K.F. Hua, Y.C. Lin, et al., IL-36 signaling facilitates activation of the NLRP3 inflammasome and IL-23/IL-17 Axis in renal inflammation and fibrosis, J. Am. Soc. Nephrol. : JASN (J. Am. Soc. Nephrol.) 28 (7) (2017) 2022–2037.

[55] I. Ludwig-Portugall, E. Bartok, E. Dhana, et al., An NLRP3-specific inflammasome inhibitor attenuates crystal-induced kidney fibrosis in mice, Kidney Int. 90 (3) (2016) 525–539.

[56] Q. Chen, S. Yu, K. Zhang, et al., Exogenous H2S inhibits autophagy in unilateral ureteral obstruction mouse renal tubule cells by regulating the ROS-AMPK signaling pathway, Cell. Physiol. Biochem. : Int. J. Exp. Cell. Physiol. Biochem. pharmacol. 49 (6) (2018) 2200–2213.

[57] I. Lobb, M. Davison, D. Carter, et al., Hydrogen sulfide treatment mitigates renal allograft ischemia-reperfusion injury during cold storage and improves early transplant kidney function and survival following allogeneic renal transplantation, J. Urol. 194 (6) (2015) 1806–1815.

[58] Q. Ling, X. Yu, T. Wang, S.G. Wang, Z.Q. Ye, J.H. Liu, Roles of the exogenous H2S-mediated SR-A signaling pathway in renal ischemia/reperfusion injury in regulating endoplasmic reticulum stress-induced autophagy in a rat model, Cell. Physiol. Biochem. : Int. J. Exp. Cell. Physiol. Biochem. pharmacol. 41 (6) (2017) 2461–2474.

[59] D. Wu, N. Luo, L. Wang, et al., Hydrogen sulfide ameliorates chronic renal failure in rats by inhibiting apoptosis and inflammation through ROS/MAPK and NF-kappaB signaling pathways, Sci. Rep. 7 (1) (2017) 455.

[60] D. Wu, B. Gao, M. Li, et al., Hydrogen sulfide mitigates kidney injury in high fat diet-induced obese mice, Oxidative Med. Cell. Longev. 2016 (2016) 2715718.